# Macrophage-derived CCL1 targets CCR8 receptor in hepatic stellate cells to promote liver fibrosis through JAk/STAT pathway

**Jun Li** ( lj@ahmu.edu.cn )
Anhui Medical University https://orcid.org/0000-0001-7541-752X
**Shaoxi Diao**
Anhui Medical University
**Liangyun Li**
Anhui Medical University
**Jintong Zhang**
Anhui Medical University
**Minglu Ji**
Anhui Medical University
**Lijiao Sun**
Anhui Medical University
**Wen-wen Shen**
Anhui Medical University
**Shuai Wu**
Anhui Medical University
**Zixiang Chen**
The First Affiliated Hospital of Anhui Medical University
**Cheng Huang**
Anhui Provincial laboratory of inflammatory and immunity disease https://orcid.org/0000-0003-2208-2505

**Article**

**Keywords:** Liver fibrosis, C-C motif chemokine ligand 1, C-C motif chemokine receptor 8, JAK/STAT pathway, apoptosis

**Posted Date:** January 12th, 2024

**DOI:** https://doi.org/10.21203/rs.3.rs-3723244/v1

**Additional Declarations:** (Not answered)

---

# Abstract

Liver fibrosis is caused by liver injury resulting from the wound healing response. According to recent research, the primary factor responsible for liver fibrosis is the activation of hepatic stellate cells (HSCs). C-C motif chemokine ligand 1 (CCL1) is one of several chemokine genes clustered on chromosome 17, which is involved in immune regulation and inflammatory processes. However, the role of CCL1 in liver fibrosis has not been reported. We found that CCL1 secreted by macrophages can target and activate the receptor protein C-C motif chemokine receptor 8 (CCR8) of HSCs, accelerating liver fibrosis progression by activating the Janus kinase (JAK)/signal transducer and activator of transcription (STAT) signalling pathway. This suggested that the CCL1-mediated regulation of CCR8 is an important event in liver fibrosis progression. In conclusion, this study identified a novel signalling axis, the CCL1/CCR8/JAK/STAT pathway, which regulates the activation and apoptosis of HSCs, thus providing a novel therapeutic strategy for liver fibrosis.


# 1. Introduction

Liver fibrosis is a chronic inflammatory injury of the liver that triggers a sustained damage repair response, leading to abnormal deposition of extracellular matrix (ECM) in the liver tissue. The aggravation of liver fibrosis further triggers a pathological process of abnormal changes in the structure and function of liver, eventually transforming into cirrhosis, necrosis, and liver cancer[1]. Hepatic stellate cells (HSCs), which are the main host cells, play an important role in liver fibrosis response. Both the activation and apoptosis of HSCs play a crucial role in liver fibrosis[3],influencing chemokines, cytokines, and some regulation of the increase of the cells, cytokines, and chemokines, and are resident mostly in the liver cells[4–6]. During fibrosis, HSCs transition from a resting to an activated state and secrete large amounts of ECM proteins instead of storing vitamin A. Consequently, inflammation caused by chronic hepatocyte injury leads to the accumulation of a large number of macrophages, T-cells, and dendritic cells in the liver[2].

Macrophages are intrinsically immunogenic and receive signals from the local microenvironment to promote functional differentiation. The study of macrophage heterogeneity has important implications for delineating the liver immunological status in disease and health and role of macrophages in liver inflammation treatment[7]. Chemokines are a group of small proteins that are crucial for immune and inflammatory responses[8]. Apart from facilitating leukocyte movement, they also influence blood vessels, collagen production, and the proliferation of precursor cells in the blood. The significant role of chemokines in polarised immune responses has been well-established[9]. C-C motif chemokine ligand 1 (CCL1), which has anti-apoptotic activity, was reported to induce resistance to antineoplastic drugs by activating the ERK/MAPK cascade through its interaction with the C-C motif chemokine receptor 8 (CCR8)[10] which recruits immune cells to sites of injured and inflamed tissue, thus regulating tissue homeostasis[11]. Therefore, CCL1 and CCR8 play important roles in many human inflammatory diseases[11]. CCL1 triggers the AMFR-SPRY1 pathway, promotes the differentiation of pulmonary

fibroblasts into myofibroblasts, and drives pulmonary fibrosis[12]. Thus, CCL1 plays an indispensable role in inflammation and fibrosis. As liver fibrosis is a chronic inflammatory and fibrotic process, we sought to determine the role of CCL1 in its development.

Interestingly, the expression of CCL1 was found to be elevated in the liver tissues of patients with liver fibrosis. We thus hypothesized that CCL1 plays a role in aggravating or promoting the progression of liver fibrosis in humans and mice. Therefore, we sought to explore the expression of CCL1 in a carbon tetrachloride (CCl4)-induced liver fibrosis mice model and its effect on HSCs. By studying the role of CCL1 in fibrosis we aimed to identify a new signalling pathway in liver fibrosis and provide new ideas for the development of novel drugs and treatments of liver fibrosis.

## 2. Materials and methods

## 2.1 Establishment of liver fibrosis model mice

C57BL/6J male mice aged 8 weeks and weighing 20–22 g were purchased from GemPharmatech Biotechnology Co., Ltd. (Nanjing, China). All animal experiments were approved by the Science and Technology Committee of Anhui Medical University Animal Protection and Utilization Committee. Mice in the CCl4 model group (n = 6) were intraperitoneally injected with 10% CCl4 (0.1 mL/kg) twice a week, whereas the control group (n = 6) was injected with the same amount of olive oil. After four weeks of routine feeding, mice were euthanized via neck dislocation.

## 2.2 Human liver samples

Human liver samples with liver fibrosis were collected at the Department of Hepatobiliary Surgery, the First Affiliated Hospital of Anhui Medical University (Anhui, China). All volunteers to provide samples of knowledge and agreed to the experiment, at the same time this research through the approval of the first affiliated hospital of anhui medical university. The collection of 8 cases of nonalcoholic fatty hepatitis (NASH) in patients with cirrhosis of liver fibrosis organization and liver tissue after resection of liver hemangioma patient's health. Liver tissues from 8 cirrhotic patients with non-alcoholic steatohepatitis (NASH) and 8 healthy liver tissues from patients with hepatic hemangioma were collected. The liver tissues were embedded in paraffin and frozen in liquid nitrogen for subsequent experiments.

## 2.3 Adeno-associated virus (AAV)-mediated knockdown of *CCL1*

AAV-8-Luc-F4/80-CCL1 (NM_011329.3) and AAV8-F4/80-Luc-NC cells were obtained from Hanbio Biotechnology(Shanghai,China). The different experimental groups in the Liver fibrosis in mice model is established by intraperitoneal injection, adeno-associated virus by tail vein injection in mice.Briefly, 24 healthy mice with body weights within the normal range were randomly selected and divided into four groups: control; 10% CCl4; 10% CCl4 + AAV8-Luc-NC; and 10% CCl4 + AAV-8-Luc-F/80-shCCL1. Viral infiltration in the liver of mice was detected using imaging methods.

## 2.4 Alanine aminotransferase (ALT)/aspartate aminotransferase (AST) activity

Collecting blood in mice, let stand for 4 h after 4500 RPM, 30 min centrifugal, collect serum.The serum levels of AST and ALT were measured using a Mindray BS-370 automatic biochemical analyser (IFCC method) (Shanghai Mindray Company).

## 2.5 Histopathology, immunohistochemistry (IHC), and histological staining

Paraffin section on the liver after dewaxing, using EDTA repair liquid (Beyotime, P0085, Shanghai, China) antigen repair after use with 5% bovine serum albumin (bovine serum albumin, BSA) citrate buffer to extract antigen, closed cell. The mice were then treated with anti-CCL1 antibody (1:100). Alpha sma (1 0; CST, USA) overnight at 4°C. Finally, the sections were stained with 3,3 '-diaminobenzidine tetrahydroammonium chloride, incubated at 25°C for 60 min, stained with DAPI(Beyotime) for 5 min, and observed under a microscope.

## 2.6 TUNEL staining

Mice liver tissue sections were dried in an oven at 65°C for 2 h and de-paraffinised in xylene, followed by antigen repair with an antigen repair solution using a microwave oven. After cooling to 25°C, sections were treated with 1% Triton X-100 for 10 min, washed thrice with phosphate-buffered saline (PBS), blocked with 5% BSA for 30 min, and washed thrice with PBS. Sections were incubated with DESMIN(ab32362,abcam) primary antibody(1:200) overnight at 4°C. Subsequently, sections were stained with green fluorescence-tagged secondary antibodies and TUNEL detection solution (red), and then washed thrice with PBS. Finally, DAPI (Beyotime, Shanghai, China) stain was added and incubated for 5 min, and the slides were sealed. An inverted fluorescence microscope was used to observe the two fluorescent signals and determine whether convergence occurred.

## 2.7 Immunofluorescence staining (IF)

After de-paraffinization and antigen repair, sections were blocked with 5% BSA for 30 min at 25°C. Subsequently, anti-CCL1 (1:200) and F4/80 (1:200) antibodies were added and incubated overnight at 4°C. Sections were also incubated with CCR8 (1:200) and α-SMA (1:200) antibodies overnight in the same way. Sections were then incubated with the corresponding fluorescently labelled secondary antibody for 2 h at 25°C in the dark. After 5 min at 25°C with DAPI, sections were observed under an inverted fluorescence microscope (OLYMPUS IX83, Tokyo, Japan).

## 2.8 Cell culture

RAW246.7 and LX-2 cells were purchased from the Shanghai Institute of the Chinese Academy of Sciences and cultured in DMEM (Gibco, Grand Island, NY, USA) supplemented with 10% foetal bovine

serum (Gibco) at 37°C in a humidified atmosphere of 5% $CO_2$. RAW246.7 cells were stimulated with IL-4 (40 ng/mL) for 24 h and then transformed into M2 macrophages.

## 2.9 Transient transfection of LX-2 cells

For this assay, LX-2 cells at a density of 40–50% were transfected with human GV658-CCR8 (NM_005201.4, GeneChem, Shanghai, China) using Lipofectamine™ 2000 (Invitrogen, Carlsbad, CA, USA). siRNA and negative control were transfected into activated LX-2 cells in the same manner.After 6 h, the medium was replaced with fresh high-glucose medium (10% serum); after 48 h, cells were used for subsequent experiments. All experiments were repeated three times. Cells were transfected with CCR8 shRNA (GenePharma, Shanghai, China) in a similar manner to silence the expression of CCR8. The sequences used for transient transfections are listed in Table 1.

## 2.10 RNA extraction and quantitative real-time PCR (RT-qPCR)

Mice livers were immersed in TRIzol (Invitrogen) reagent and ground to extract total RNA, which was reverse-transcribed into cDNA using a Takara kit (Accurate Biology, China). The mRNA levels of CCL1, CCR8, α-SMA, and COL-I were detected via RT-qPCR. GAPDH mRNA was used as an internal control. The primers used are listed in Table 2. Briefly, qRT-PCR was performed using Premix EX Taq (Accurate Biotechnology) on a CFX96 RT-qPCR system (Bio-Rad, California ,USA). The levels of mRNA expression of target genes were normalised against those of *GAPDH*.

## 2.11 Co-immunoprecipitation (Co-IP)

Co-IP experiments were performed to explore the binding between the CCL1 and CCR8 proteins. The lysates of RAW246.7 and LX-2 cells were extracted, and immunoprecipitation experiments were performed with CCL1 and CCR8 antibodies using a Co-IP Kit (Absin, Shanghai, China) After boiling 5 μg of immune complexes in SDS sample buffer for 10 min, the co-precipitate was electrophoresed on an SDS-PAGE denaturing gel, the bottom sample band was excised, and the remaining bands were used in the subsequent experiment.

## 2.12 Western blot

Proteins from liver tissues and LX-2 cells were lysed in RIPA and PMSF buffer at a ratio of 100:1. The protein concentration was determined using a BCA Protein Kit (Thermo Fisher Scientific, China). Equal amounts of protein were electrophoresed by SDS-PAGE and then transferred to PVDF membranes, which were blocked with 5% skim milk powder for 2 h at 25°C. Subsequently, membranes were incubated with primary antibodies against β-actin (#4970s, CST), CCL1 (PK13291, Abmart, Shanghai), α-SMA (#19245S, CST), COL-I (TA7001, Abmart), Bax (T40051, Abmart), Bcl-2 (T40056, Abmart), STAT3 (# 9139S, CST), JAK3 (ab45141, Abcam), phospho-JAK3 (5031s, CST), phospho-STAT3 (#9145S, CST), and CCR8 (T57058, Abmart) overnight at 4°C. Membranes were then washed thrice in TBST for 5 min each time and incubated with the respective secondary antibodies for 1 h at 25°C. Protein bands were detected using

electrochemiluminescence. Subsequent visualisation was performed using the ImageJ software (NIH, Bethesda, MD, USA).

## 2.13 Flow cytometry

Cells were washed thrice with TBS, digested by adding 1 mL of trypsin without EGTA, collected in EP tubes, and centrifuged at 220g for 5 min. Then, 5 μL PerCP5.5 and 5μL Annexin V-APC were added to each tube and incubated for 10 min. Apoptosis was measured using flow cytometry (Beckman Coulter, USA).

## 2.14 LV-CCL1-shCCL1-infected RAW264.7

Approximately 3–5 × $10^4$ RAW246.7 cells per mL was inoculated in each well of 96-well plates. MOI gradients were set according to MOI of 1, 10, 50, 100, and then complete medium containing a final concentration of approximately 8 μg/mL polybrene (Cat. TA003) was diluted to 100 μL. The supernatant was removed, a different MOI was used, and the culture was continued. After 24 h, the liquid was changed, and the fluorescence signal intensity was detected after 72 h. At a MOI of 50, the cell state was not affected, and the infection efficiency was approximately 80%. Among the three lentiviral sequences, AV-CCL1-shRNA1 was selected as the final sequence. Formal transfection was performed when cells reached 20–30% confluence (Table 1). Cells were treated with MOI = 50, and polybrene was added to a final concentration of 8 μg/mL. Cells were then incubated at 37°C overnight with gentle shaking. The culture medium containing the virus was removed 24 h after infection and replaced with fresh complete culture medium; purinomycin was added, transfected cells were screened out, and the culture continued at 37°C. Fluorescence was observed 72 h later, RNA was extracted, and the expression of the target genes was detected at the mRNA level.

## 2.15 Extraction of BMDM cells

After anaesthesia, mice were sacrificed via neck dislocation and placed in a beaker containing 75% ethanol to remove the foot joints and skin. The roots of the hind limbs of mice were removed, and muscle tissues were removed and placed in a Petri dish in 75% ethanol. Calf bones were transferred and soaked in cold PBS. Both ends of the femur and tibia were cut, and the bone marrow was blown out of the femur and tibia by sucking cold induction medium with a 1 mL syringe three times. The medium containing bone marrow was repeatedly blown, filtered through a 70 μm filter, transferred to a 15 mL centrifuge tube, centrifuged at 1500 rpm for 5 min, and the supernatant was discarded. Red blood cell lysis buffer was added, resuspended for 5 min, and centrifuged at 1500 rpm for 5 min. The supernatant was discarded, resuspended in precooled complete medium supplemented with M-CSF stimulating factor, and plated. The medium was not replaceable during cell growth, and cells were not passaged; half of the fresh medium containing M-CSF was replaced on the third day and completely replaced on the fifth day, and subsequent experiments were performed one week later

## 2.16 Extraction of Kupffer cells

Mice were anaesthetised, and the portal and vena cava veins were exposed. Preheated HBSS (50 mL/mouse) was infused through the portal vein. The inferior vena cava was excised. Approximately 45 mL of HBSS was replaced with collagenase digestion solution (70–80 mL), perfusion was continued, and the livers were excised intact and placed in Petri dishes containing the medium. Kupffer was released into the suspension by shaking the liver from the rupture and filtered through a 100 μm screen. Samples were centrifuged at 50 × *g* for 2 min at 4°C. The supernatants were collected; this was repeated twice. The supernatant was collected and centrifuged at 1350 × *g* for 15 min at 4°C. The supernatant was removed, and liver non-parenchymal cells were precipitated with 10 mL of medium. Percoll density gradient separation solutions of 25 and 50% were prepared. A 50% Percoll solution was spread on the bottom, followed by a 25% Percoll solution and, finally, a liver non-parenchymal cell suspension. Cells were centrifuged at 850 × *g* for 15 min at 4°C. Kupffer cells with 25 to 50% Percoll were collected, transferred to new tubes, 35–40 mL medium was added and centrifuged at 1350 × *g* for 15 min at 4°C. The supernatant was discarded, and cells were resuspended in 5–10 mL of pre-warmed medium, spread, and incubated for 30 min at 37°C in a 5% $CO_2$ incubator. The supernatant was discarded, cells were washed with HBSS, and the medium was replaced with fresh medium.

## 2.17 Cell Counting Kit-8 (CCK-8) assay

CCK-8 was used to detect the proliferation of LX-2 cells. LX-2 cells were evenly distributed in 96-well plates. Then, 10 μL of CCK-8 reagent was added to each well. The plates were incubated for 2 h in a constant temperature incubator at 37°C. In the control group, 100 μL of DMSO was added to each well, and absorbance was measured at 450 nm. Cell viability (%) was calculated using the following formula: (measured value - blank value)/(control value - blank value) × 100%.

## 2.18 ELISA

An ELISA kit (JYM1155Mo, Colorful Gene Biotech, Wuhan, China) was used to detect the expression of CCL1 in the serum of mice in different groups. A gradient dilution of standards was first completed in 96-well plates, according to the manufacturer's instructions. Blank control wells were set up, and 10 μL of serum samples was added to each well after the addition of 40 μL of diluent. Subsequently, except for blank wells, 50 μL of the enzyme-labelled reagent was added to each well, sealed with plate sealing membrane and incubated at 37°C for 30 min. After the sealing plate film was removed, the liquid was discarded, dried, filled with washing solution and washed five times for 30 s each time. Then, 50 μL of chromogen was added to each well, and the mixture was mixed with shaking and incubated at 37°C for 10 min in the dark. Absorbance was measured at 450 nm.

## 2.19 Inhibition of the STAT3 pathway

Using concentration for 10 um Stattic (purchased from Selleck, Texas, USA) added to the density of 50% − 60% LX − 2 cells, culture collection cells extracted after 48 h protein, after determine the inhibition of STAT3 effects respectively to test the HSC activation index.

## 2.20 Statistical analysis

The Student's *t*-test was used to compare differences between two groups. One-way ANOVA was used to compare differences among multiple groups. (Prism 8.0 GraphPad Software, USA). The data are presented as the mean ± SEM. A $P < 0.05$ was considered statistically significant.

# 3. Results

## 3.1 CCL1 upregulation in liver fibrosis

Of note, H&E and Masson staining revealed extensive fibrous depositions in liver fibrotic tissues. In addition, IHC staining revealed a notable upregulation of the expression of CCL1 in liver fibrotic tissues (Fig. 1a). Western blotting and RT-qPCR revealed that the expression of CCL1 in fibrotic liver tissues was significantly higher than that in normal liver tissues (Fig. 1b, c). Interestingly, CCL1 (green) was mainly localised to F4/80(red)-labelled macrophages in the liver tissues of mice with liver fibrosis (Fig. 1d). We also detected the expression of CCL1 in Kupffer cells extracted from mice with liver fibrosis and normal mice using RT-qPCR and western blot analyses. We accordingly found that the expression of CCL1 was upregulated in the model group (Fig. 1e,g). We further explored the serum levels of CCL1 in the model group and normal group using an ELISA kit, and found that the expression of CCL1 was upregulated in the model group (Fig. 1f). Western blot and RT-qPCR analyses showed that the level of apoptosis in LX-2 cells treated with TGF-β was significantly decreased. The TUNEL kit also showed similar results (Fig. 1h). Taken together, these results indicated that CCL1 is mainly localised in liver macrophages, and that its expression is increased in fibrotic liver tissues.

## 3.2 Successful *in vivo* model of liver fibrosis

Figure 2a shows the establishment of a CCl4-induced mouse liver fibrosis model. Compared with the control group, the liver tissue of mice in the CCl4-treated group showed obvious pathological changes, characterized by significantly extended fibrosis, voids, and steatosis. The liver fibrosis group was also characterised by inflammatory cells and disturbances in the lobular structure, whereas such infiltration and lesions were seldom observed in the control group. Masson and Sirius red staining showed significant collagen deposition in the CCl4 group, but significantly less collagen deposition in the control group. We also noticed that the serum levels of ALT and AST in the CCl4 group were significantly higher than those in the normal group (Fig. 2c). In addition, IHC revealed a significant increase in the expression of CCL1 (Fig. 2b). Both protein and mRNA levels showed that the HSC activation index was significantly upregulated, whereas apoptosis was downregulated in mice with liver fibrosis (Fig. 2d,e). Furthermore, IF of mouse liver sections revealed increased levels of Desmin but inhibited apoptosis in mice with liver fibrosis (TUNEL) (Fig. 2f). Finally, we found that the expression of CCL1 was upregulated in liver tissues during fibrosis. Hence, we successfully established a mouse model of liver fibrosis.

## 3.3 Liver macrophage-specific AAV8-Luc-F4/80-CCL1 knockdown reduced liver fibrosis

Although CCL1 is upregulated in liver fibrosis, CCL1 was knocked down in mice after systemic administration of AAV8-Luc-F4/80-CCL1 (AAV specifically localised to the promoter of murine liver macrophages), showing effective liver-specific transduction. Both AAV8-F4/80-Luc-empty and AAV8–F4/80-Luc-CCL1 were successfully delivered into the liver via tail vein injection as shown using small animal *in vivo* imaging (Fig. 3a). H&E staining revealed abnormal hyperplasia of the connective tissue in the liver, dysfunction of the hepatic cords, hyperplasia of fibroblasts around the pseudolobules, and decreased lymphocyte infiltration in mice with liver fibrosis in the CCl4 control group (Fig. 3b). However, liver fibrosis was significantly decreased in the AAV–shCCL1 group. Masson and Sirius Red staining demonstrated that AAV8-shCCL1 effectively alleviated liver fibrosis, decreased inflammatory cell infiltration, and inhibited fibroblast proliferation in mice. IHC results showed that the level of α-SMA in the liver tissue of the AAV8-shCCL1 group was significantly lower than that in the AAV8-NC group (Fig. 3b). The levels of AST and ALT in normal liver tissue and CCl4 liver tissue were similar to those in the previous model, whereas those in the AAV-shCCL1 group were significantly lower than those in the AAV-NC group (Fig. 3c). Western blotting and RT-qPCR revealed that treatment with AAV8-CCL1 effectively suppressed the CCl4-induced elevation in the levels of α-SMA and COL-I, as well as Bax/Bcl-2 (Fig. 3d, e). The results of TUNEL and Desmin double staining in mice liver sections showed that the selective knockdown of *CCL1* using AAV-shCCL1 reduced the expression of Desmin, whereas increased the level of apoptosis in macrophages (Fig. 3f). Analysis of CCL1 (red) and F4/80 (green)-stained mice liver tissues showed that AAV-shCCL1 successfully knocked down the expression of CCL1 in macrophages in liver fibrosis model mice (Fig. 3g). In conclusion, AAV8-Luc-F4/80-CCL1 reversed the decrease in the levels of CCL1 in CCl4-treated mice.

# 3.4 CCL1 affects HSC activation and apoptosis

We further observed that the mRNA expression of *CCL1* was significantly increased in the livers of mice with liver fibrosis; more specifically, we found that CCL1 was upregulated in the CCl4 group compared with that in the control group. To elucidate the role of CCL1 in the pathogenesis of liver fibrosis, M1 and M2 macrophages were induced via LPS and IL-4 in RAW264.7 cells, and the successful induction of M1 and M2 macrophages was detected via flow cytometry. The level of CCL1 secreted by M2 macrophages was significantly higher than that secreted by M1 macrophages. IF results showed that CCL1 co-localised with M2 macrophages (Fig. 4f). To further verify the direct effect of CCL1 on HSCs, we added exogenous recombinant CCL1 protein as a stimulus to HSC cultures. Accordingly, we observed that the levels of α-SMA and COL.I were significantly increased, whereas those of Bax/Bcl-2 were decreased, and apoptosis was inhibited after adding CCL1 (Fig. 4a, b). The CCK-8 assay showed that CCR8 overexpression decreased the level of apoptosis in LX-2 cells, whereas CCR8 knockdown increased it (Fig. 4c). The apoptosis of HSCs treated with CCL1 was significantly inhibited as shown by the 7-AAD kit and TUNEL staining (Fig. 4d, e). These data suggested that CCL1 affects the activation and apoptosis of HSCs.

# 3.5 CCR8 is a receptor for CCL1 on LX-2 cells

CCR8 has been identified as a receptor for CCL1. Of note, both CCL1 and CCR8 in humans are homologous to those in mice. Co-IP results showed that CCL1 and CCR8 were bound to each other (Fig. 5a). We found that the expression of CCR8 was reduced in the AAV-shCCL1 group compared with that in the AAV-NC group (Fig. 5b-d). We also found that CCR8 and α-SMA co-localised on LX-2 cells, suggesting that CCR8 may be involved in the activation of HSCs. To further explore the role of CCL1-CCR8, we used AAV8 to downregulate the expression of CCL1 in RAW246.7 cells, which were then co-cultured with mouse HSCs. PCR and western blot analyses showed that the expression of CCR8, α-SMA, and COL-I was downregulated in HSCs after silencing CCL1 (Fig. 5e, f). These results suggested that macrophages in the liver regulate the expression of CCR8 in HSCs by specifically secreting CCL1, thus affecting the activation and apoptosis of HSCs.

## 3.6 CCL1-CCR8 promoted HSC activation through the JAK/STAT signalling pathway

The JAK/STAT signalling pathway is crucial for the development of liver fibrosis. Recent studies highlighted the role of signal transducer and activator of transcription 3 (STAT3) in this process. STAT3 activation prevents stem cell death and facilitates fibrosis formation in HSCs. Consequently, we hypothesised that STAT3 plays a role in CCL1-induced HSC activation. Western blot analysis revealed that STAT3 phosphorylation was increased in the TGF-β-stimulated and CCR8-overexpressing groups (Fig. 6b). CCR8 overexpression upregulated the levels of the p-STAT3 protein and increased its nuclear uptake. The opposite result was obtained following transfection with CCR8 shRNA (Fig. 6a). After addition of the STAT3 inhibitor Stattic to LX-2 cells, the apoptosis level of LX-2 cells was increased, whereas the activation level was decreased (Fig. 6c). Therefore, CCL1-CCR8 probably causes liver fibrosis through the JAK-STAT signalling pathway.

# 4. Discussion

Liver fibrosis is one of the most devastating liver diseases in modern times. However, its underlying causes are unclear, hindering prevention and treatment. Liver fibrosis mostly develops in the early stages of liver cirrhosis and hepatocellular carcinoma, and treatment is favourable at this stage[13,14]. In this study, we found that CCL1, an endogenous detrimental factor, plays an important role in the development of liver fibrosis. It is secreted by macrophages after liver injury and plays an important role in HSC activation. HSCs play a crucial role as primary suppliers of collagen to the liver. They release ECM proteins, inhibit the activity of metalloproteinases, and induce the production of matrix metalloproteinases, contributing to ongoing liver structural remodeling[4,15]. Importantly, HSCs account for 80% of the total production of fibrocollagen I in fibrotic livers[16–19]. IL-6 and TGF-β have been identified as cytokines that stimulate the activation of HSCs and cause collagen secretion and deposition, and have been widely used *in vitro* to establish liver fibrosis models[20,21]. The ECM is mainly composed of fibrous scar tissue formed after massive accumulation of type I and type III collagen, which replaces normal tissue and causes liver fibrosis. The apoptosis of HSCs is inhibited (the Bax/Bcl-2 ratio decreases) during

the progression of liver fibrosis[22,23]. Therefore, activated haematopoietic stem cell depletion is essential for the resolution of fibrosis, and inhibition of CCL1 can effectively reduce liver fibrosis. Macrophages are essential immune cells in the immune system[24–27].

Monocyte-derived macrophage infiltration plays a crucial role in mouse models of liver fibrosis[28,29] and in patients with cirrhosis[30]. CCL1 acts as a chemokine by recruiting immune cells to sites of injury and inflamed tissue through its interaction with CCR8, thereby regulating tissue homeostasis[11]. Excess CCL1 can have a direct adverse effect on disease prognosis. Under different microenvironments, macrophages can be polarised into the classically activated M1 phenotype or selectively activated M2 phenotype[31]. M2 macrophages exert anti-inflammatory, tissue regeneration and repair, angiogenesis and immune regulation, phagocytosis, and tumour-modulating functions[32]. The transition between M1 and M2 macrophages is evident during infection, wound healing, and cancer[33]. Our data showed that M2 macrophages mediate CCL1 production, further affecting HSC activation. In this study, the RNA-seq data confirmed that CCL1 was specifically secreted by macrophages. *In vivo* and *in vitro* experiments confirmed that CCL1 is directly secreted by M2 macrophages and affects HSC activation, leading to collagen deposition and liver injury. In this study, we established a key link between the two, revealing that CCL1 is highly expressed in the livers of mice with liver fibrosis, and that HSCs tend to be activated upon CCL1 stimulation. In addition, silencing CCL1 significantly reduced liver collagen deposition and liver damage and alleviated liver fibrosis-related liver damage in mice with liver fibrosis. After CCL1 treatment *in vitro*, the CCR8 expression in LX-2 cells, HSC activation, α-SMA secretion, and type I collagen deposition were increased, whereas the apoptosis of LX-2 cells was inhibited. CCR8 inhibition significantly inhibited the activation of HSCs and secretion of fibrosis markers. In addition, AAV8-Luc-F4/80-CCL1 effectively alleviated CCl4-induced liver fibrosis in mice. Apoptosis of activated HSCs is a sign of the inhibition or recovery of liver fibrosis[18]. In addition, the number of TUNEL-positive HSC cells increased in the liver of *Ccl1*-knockdown mice. Therefore, we suggest that CCL1 promotes or aggravates liver fibrosis progression by activating HSCs and inhibiting apoptosis.

A database query revealed that CCL1-CCR8 usually interacts with the JAK/STAT pathway to regulate downstream genes. STAT3 is well documented for its significant contribution to liver fibrosis[34–36]. As part of the STAT family, STAT3 is primarily found in the inactive state within the cytoplasm of unstimulated cells[37,38]. Degradation of the inhibitor is required for the activation of other members of the STAT family, but not STAT3, which can directly enter the nucleus to activate relevant target genes after induced dimerisation[39,40]. STAT is mostly activated by the JAK family of tyrosine kinases, whereas STAT3 is mainly activated by JAK1[41]. The role of STAT3 *in vivo* is complex, and maintaining a balance is crucial. Its long-term activation is associated with a variety of malignant tumours, whereas its ablation can lead to abnormal development of the body[42]. Activated STAT3 and its target genes have been detected in various types of cancer[43]. STAT3 is difficult to activate naturally. Generally, it is only activated in the tumour microenvironment through long-term stimulation via extracellular signals[43]. In fact, many extracellular signals that can stimulate STAT3 activation have been found in the tumour

microenvironment, including IL-6, IL-10 family, IL-12, EGF, IL-21, IL-19, and IL-20; therefore, STAT3 is one of the most frequently activated transcription factors in cancer[44–46]. Earlier research has indicated the significant involvement of the JAK/STAT pathway in the development of liver fibrosis. During liver fibrosis, numerous extracellular factors can trigger the activation of the JAK/STAT pathway. Consequently, this activation leads to the phosphorylation and subsequent promotion of transcription of relevant target genes within the nucleus. The STAT3 pathway is activated by IL-17 to stimulate HSCs to release type I collagen and promote HSC differentiation into fibroblasts[47]. For example, miR-92b-3p activates the JAK/STAT pathway by targeting CREB3L2 to promote HSC activation and the progression of liver fibrosis[48]. However, the relationship between CCL1-CCR8 and the JAK/STAT signalling pathway in the progression of liver fibrosis remains unclear.

STAT3 signalling is the main pathway that induces the activation of fibroblasts and HSCs into myofibroblast-like cells[34,35,49]. STAT3 signalling can be activated by a variety of extracellular molecules, such as IL-6, TGF-β, and IL-10[50,51]. We found that CCL1-CCR8 promoted the expression of the p-STAT3 protein. Following the inhibition of STAT3 using the Stattic inhibitor, the activation and apoptosis of LX-2 cells was observed. The activation level of LX-2 cells was significantly decreased, whereas the apoptosis level was increased after inhibition of the JAK/STAT3 pathway. Taken together, these results demonstrated that CCL1-CCR8 regulates the progression of liver fibrosis through the JAK/STAT3 pathway. This study had several limitations. We did not use whole-body or conditional gene knockout mice, limiting the generalization of our findings. In the future, we will generate whole-body gene knockout mice for a more comprehensive research. We believe that concomitant functional verification of the effect of CCL1/CCR8 on human and mouse HSCs would have strengthened the results of our study; however, due to the limitation of time and experimental materials we could not perform this at the moment, but we will try to do so in the future. In summary, in future work, we will further improve the experimental methods and introduce gene knockout mice, and study the mechanism of action from multiple perspectives.

# Declarations

### Author contributions

X.D,L-Y.L, and J-T. Z. performed the cell experiment, analyzed the data and wrote the manuscript. M-L.J and J-L.S. provided a series of experimental instructions and help. W-W.S and S.W performed the animal experiments. J.L contributed new reagents or analytic tools. All authors approved the final version of the manuscript.

### Declaration of competing interest

The authors declare that they have no conflicts of interest.

### Data Availability

The data that has been used is confidential.

### Acknowledgments

We sincerely thank the staff of the Department of Hepatobiliary Surgery at the First Affiliated Hospital of Anhui Medical University, for their support during the study.

### Ethics approval and consent to participate

All experiments involving animals were in accordance with institutional animal welfare guidelines and approved by the Institutional Animal Care and Use Committee of Anhui Medical University (No.LLSC20190608). The study was with the approval of the Institutional Review Boards of each participating institution and conducted in accordance with the Declaration of Helsinki and Ethical Guidelines for Clinical Studies (No. 20190543). All patients provided written informed consent.

## References

1. Gao B, Bataller R. Alcoholic liver disease: Pathogenesis and new therapeutic targets. *Gastroenterology*. 2011;141:1572-1585
2. Mormone E, George J, Nieto N. Molecular pathogenesis of hepatic fibrosis and current therapeutic approaches. *Chem Biol Interact*. 2011;193:225-231
3. Li L, Diao S, Chen Z, Zhang J, Chen W, Wang T, et al. Dnmt3a-mediated methylation of tcf21/hnrnpa1 aggravates hepatic fibrosis by regulating the nf-kappab signaling pathway. *Pharmacol Res*. 2023;193:106808
4. Ogawa S, Ochi T, Shimada H, Inagaki K, Fujita I, Nii A, et al. Anti-PDGF-b monoclonal antibody reduces liver fibrosis development. *Hepatol Res*. 2010;40:1128-1141
5. Gressner AM, Weiskirchen R, Breitkopf K, Dooley S. Roles of TGF-beta in hepatic fibrosis. *Front Biosci*. 2002;7:d793-807
6. Dewidar B, Meyer C, Dooley S, Meindl-Beinker AN. TGF-beta in hepatic stellate cell activation and liver fibrogenesis-updated 2019. *Cells*. 2019;8:1419
7. Kisseleva T, Brenner D. Molecular and cellular mechanisms of liver fibrosis and its regression. *Nat Rev Gastroenterol Hepatol*. 2021;18:151-166
8. Ballardini G, Fallani M, Biagini G, Bianchi FB, Pisi E. Desmin and actin in the identification of Ito cells and in monitoring their evolution to myofibroblasts in experimental liver fibrosis. *Virchows Arch B Cell Pathol Incl Mol Pathol*. 1988;56:45-49
9. Failli P, De FR, Caligiuri A, Gentilini A, Romanelli RG, Marra F, et al. Nitrovasodilators inhibit platelet-derived growth factor-induced proliferation and migration of activated human hepatic stellate cells. *Gastroenterology*. 2000;119:479-492
10. Krenkel O, Tacke F. Liver macrophages in tissue homeostasis and disease. *Nat Rev Immunol*. 2017;17:306-321

11. Rollins BJ. Chemokines. *Blood*. 1997;90:909-928
12. Mantovani A. The chemokine system: Redundancy for robust outputs. *Immunol Today*. 1999;20:254-257
13. Marra F, Tacke F. Roles for chemokines in liver disease. *Gastroenterology*. 2014;147:577-594e571
14. Korbecki J, Grochans S, Gutowska I, Barczak K, Baranowska-Bosiacka I. CC chemokines in a tumor: A review of pro-cancer and anti-cancer properties of receptors CCR5, CCR6, CCR7, CCR8, CCR9, and CCR10 ligands. *Int J Mol Sci*. 2020;21:7619
15. Gombert M, Dieu-Nosjean MC, Winterberg F, Bunemann E, Kubitza RC, Da Cunha L, et al. CCL1-CCR8 interactions: An axis mediating the recruitment of t cells and langerhans-type dendritic cells to sites of atopic skin inflammation. *J Immunol*. 2005;174:5082-5091
16. Liu SS, Liu C, Lv XX, Cui B, Yan J, Li YX, et al. The chemokine CCL1 triggers an AMFR-SPRY1 pathway that promotes differentiation of lung fibroblasts into myofibroblasts and drives pulmonary fibrosis. *Immunity*. 2021;54:2042-2056e2048
17. Darnell JE, Jr., Kerr IM, Stark GR. JAK-STAT pathways and transcriptional activation in response to IFNS and other extracellular signaling proteins. *Science*. 1994;264:1415-1421
18. Yu H, Jove R. The stats of cancer--new molecular targets come of age. *Nat Rev Cancer*. 2004;4:97-105
19. Braunstein J, Brutsaert S, Olson R, Schindler C. Stats dimerize in the absence of phosphorylation. *J Biol Chem*. 2003;278:34133-34140
20. Yang J, Liao X, Agarwal MK, Barnes L, Auron PE, Stark GR. Unphosphorylated STAT3 accumulates in response to IL-6 and activates transcription by binding to NFkappaB. *Genes Dev*. 2007;21:1396-1408
21. Hirano T, Ishihara K, Hibi M. Roles of STAT3 in mediating the cell growth, differentiation and survival signals relayed through the IL-6 family of cytokine receptors. *Oncogene*. 2000;19:2548-2556
22. Takeda K, Noguchi K, Shi W, Tanaka T, Matsumoto M, Yoshida N, et al. Targeted disruption of the mouse stat3 gene leads to early embryonic lethality. *Proc Natl Acad Sci U S A*. 1997;94:3801-3804
23. Grivennikov SI, Karin M. Dangerous liaisons: STAT3 and NF-kappaB collaboration and crosstalk in cancer. *Cytokine Growth Factor Rev*. 2010;21:11-19
24. Darnell JE, Jr. Transcription factors as targets for cancer therapy. *Nat Rev Cancer*. 2002;2:740-749
25. Ghoreschi K, Laurence A, O'Shea JJ. Janus kinases in immune cell signaling. *Immunol Rev*. 2009;228:273-287
26. Yang J, Chatterjee-Kishore M, Staugaitis SM, Nguyen H, Schlessinger K, Levy DE, et al. Novel roles of unphosphorylated STAT3 in oncogenesis and transcriptional regulation. *Cancer Res*. 2005;65:939-947
27. Meng F, Wang K, Aoyama T, Grivennikov SI, Paik Y, Scholten D, et al. Interleukin-17 signaling in inflammatory, Kupffer cells, and hepatic stellate cells exacerbates liver fibrosis in mice. *Gastroenterology*. 2012;143:765-776 e763

28. Huang W, Ji R, Ge S, Zhou D, Liu Z, Sun Y, et al. Microrna-92b-3p promotes the progression of liver fibrosis by targeting CREB3L2 through the JAK/STAT signaling pathway. *Pathol Res Pract*. 2021;219:153367
29. Zong Z, Liu J, Wang N, Yang C, Wang Q, Zhang W, et al. Nicotinamide mononucleotide inhibits hepatic stellate cell activation to prevent liver fibrosis via promoting PGE(2) degradation. *Free Radic Biol Med*. 2021;162:571-581
30. Ramachandran P, Iredale JP. Liver fibrosis: A bidirectional model of fibrogenesis and resolution. *QJM*. 2012;105:813-817
31. Moreira RK. Hepatic stellate cells and liver fibrosis. *Arch Pathol Lab Med*. 2007;131:1728-1734
32. Lepreux S, Desmouliere A. Human liver myofibroblasts during development and diseases with a focus on portal (myo)fibroblasts. *Front Physiol*. 2015;6:173
33. Li D, He L, Guo H, Chen H, Shan H. Targeting activated hepatic stellate cells (aHSCs) for liver fibrosis imaging. *EJNMMI Res*. 2015;5:71
34. Puche JE, Saiman Y, Friedman SL. Hepatic stellate cells and liver fibrosis. *Compr Physiol*. 2013;3:1473-1492
35. Rao HY, Wei L, Li J, Zhang LF, Chen HY, Zhu LM, et al. Liver fibrosis and hepatic stellate cells improvement of chronic hepatitis c patients by interferon-beta-1a with or without sustained viral response. *Hepatogastroenterology*. 2009;56:328-334
36. Emami CN, Mittal R, Wang L, Ford HR, Prasadarao NV. Role of neutrophils and macrophages in the pathogenesis of necrotizing enterocolitis caused by Cronobacter sakazakii. *J Surg Res*. 2012;172:18-28
37. Gourlay DM. The good and the bad of the innate immune response in necrotizing enterocolitis. *J Surg Res*. 2012;175:51-53
38. Li C, Qu L, Farragher C, Vella A, Zhou B. Microrna regulated macrophage activation in obesity. *J Transl Int Med*. 2019;7:46-52
39. Li C, Qu L, Matz AJ, Murphy PA, Liu Y, Manichaikul AW, et al. Atherospectrum reveals novel macrophage foam cell gene signatures associated with atherosclerotic cardiovascular disease risk. *Circulation*. 2022;145:206-218
40. Duffield JS, Forbes SJ, Constandinou CM, Clay S, Partolina M, Vuthoori S, et al. Selective depletion of macrophages reveals distinct, opposing roles during liver injury and repair. *J Clin Invest*. 2005;115:56-65
41. Karlmark KR, Weiskirchen R, Zimmermann HW, Gassler N, Ginhoux F, Weber C, et al. Hepatic recruitment of the inflammatory GR1+ monocyte subset upon liver injury promotes hepatic fibrosis. *Hepatology*. 2009;50:261-274
42. Zimmermann HW, Seidler S, Nattermann J, Gassler N, Hellerbrand C, Zernecke A, et al. Functional contribution of elevated circulating and hepatic non-classical CD14CD16 monocytes to inflammation and human liver fibrosis. *PLoS One*. 2010;5:e11049

43. Sica A, Mantovani A. Macrophage plasticity and polarization: In vivo veritas. *J Clin Invest*. 2012;122:787-795
44. Yao Y, Xu XH, Jin L. Macrophage polarization in physiological and pathological pregnancy. *Front Immunol*. 2019;10:792
45. Hidalgo-Garcia L, Galvez J, Rodriguez-Cabezas ME, Anderson PO. Can a conversation between mesenchymal stromal cells and macrophages solve the crisis in the inflamed intestine? *Front Pharmacol*. 2018;9:179
46. Chen L, Zhuo HZ, Wu JY, Lin LY, Huang ZL, Lu JX, et al. Mir-92b inhibits proliferation and invasion of lung cancer by targeting EZH2. *Eur Rev Med Pharmacol Sci*. 2020;24:3166-3173
47. Ni QF, Zhang Y, Yu JW, Hua RH, Wang QH, Zhu JW. Mir-92b promotes gastric cancer growth by activating the DAB2IP-mediated PI3K/AKT signalling pathway. *Cell Prolif*. 2020;53:e12630
48. Zhang W, Duan W, Mo Z, Wang J, Yang W, Wu W, et al. Upregulation of SNHG14 suppresses cell proliferation and metastasis of colorectal cancer by targeting mir-92b-3p. *J Cell Biochem*. 2020;121:1998-2008
49. Su Q, Li L, Zhao J, Sun Y, Yang H. Mirna expression profile of the myocardial tissue of pigs with coronary microembolization. *Cell Physiol Biochem*. 2017;43:1012-1024
50. Yuchuan H, Ya D, Jie Z, Jingqiu C, Yanrong L, Dongliang L, et al. Circulating miRNAs might be promising biomarkers to reflect the dynamic pathological changes in smoking-related interstitial fibrosis. *Toxicol Ind Health*. 2014;30:182-191
51. Hao X, Ma C, Chen S, Dang J, Cheng X, Zhu D. Reverse the down regulation of mir-92b-3p by hypoxia can suppress the proliferation of pulmonary artery smooth muscle cells by targeting USP28. *Biochem Biophys Res Commun*. 2018;503:3064-3077

# Tables

Table.1 The sequences used in transient transfection analysise

| Gene | Sense (5'-3') | Antisense (5'-3') |
|---|---|---|
| CCL1-shRNA 1 | GCATGCTTACGGTCTCCAATA | TATTGGAGACCGTAAGCATGC |
| CCL1-shRNA2 | CTGAAGTTTATCCAGTGTTAC | GTAACACTGGATAAACTTCAG |
| CCL1-shRNA3 | TGGTATTCAGGCTGAACAAAG | CTTTGTTCAGCCTGAATACCA |
| CCR8 siRNA | GAAGACGGCAUGCUACAAUTT | AUUGUAGCAUGCCGUCUUCTT |
| GV648-CCR8 | GGAUGAGUCCAUCAAGGAATT | UUCCUUGAUGGACUCAUCCTT |
| Scrambled-RNAi | UUCUCCGAACGUGUCACGUTT | ACGUGACACGUUCGGAGAATT |
| AAV8-CCL1-shRNA | ccCGAGAGTGACCTGAAAGAA | TTCTTTCAGGTCACTCTCGGG |

Table.2 Primers used in RT-qPCR

| Gene | Forward Primer (5'-3') | Reverse Primer (3'-5') |
|---|---|---|
| human | | |
| β-actin | GCCAACACAGTGCTGCTGG | CTCAGGAGGAGCAATGATCTTG |
| α-SMA | GTGTTGCCCCTGAAGAGCAT | GCTGGGACATTGAAAGTCTCA |
| Col1α1 | GAGGGCCAAGACGAAGACATC | CAGATCACGTCATCGCACAAC |
| BAX | CCCGAGAGGTCTTTTTCCGAG | CCAGCCCATGATGGTTCTGAT |
| BCL-2 | TGGGGCGGATCTTCTGTGA | GTGACCAGCGTGGGATACTG |
| CCL1 | TCCTGGCTAACGACAAATACGA | TTTCCCGGCCACCATAAAGG |
| CCR8 | TCAGAGTCTCCTAAAGAGCCC | ACCTTGTGTGGCCTTGCAT |
| mouse | | |
| β-actin | GCCAACACAGTGCTGTCTGG | CTCAGGAGGAGCAATGATCTTG |
| α-SMA | CCCAGACATCAGGGAGTAATG | TCTATCGGATACTTCAGCGTCA |
| Col1α1 | GCTCCTCTTAGGGGCCACT | ATTGGGGACCCTTAGGCCAT |
| BAX | AGACAGGGGCCTTTTTGCTAC | AATTCGCCGGAGACACTCG |
| BCL-2 | GCTACCGTCGTGACTTCGC | CCCCACCGAACTCAAAGAAGG |
| CCL1 | TGCCGTGTGGATACAGGATG | GTTGAGGCGCAGCTTTCTCTA |
| CCR8 | ACGTCACGATGACCGACTACT | ACGAGGACTAAGATGACCAGG |

# Figures

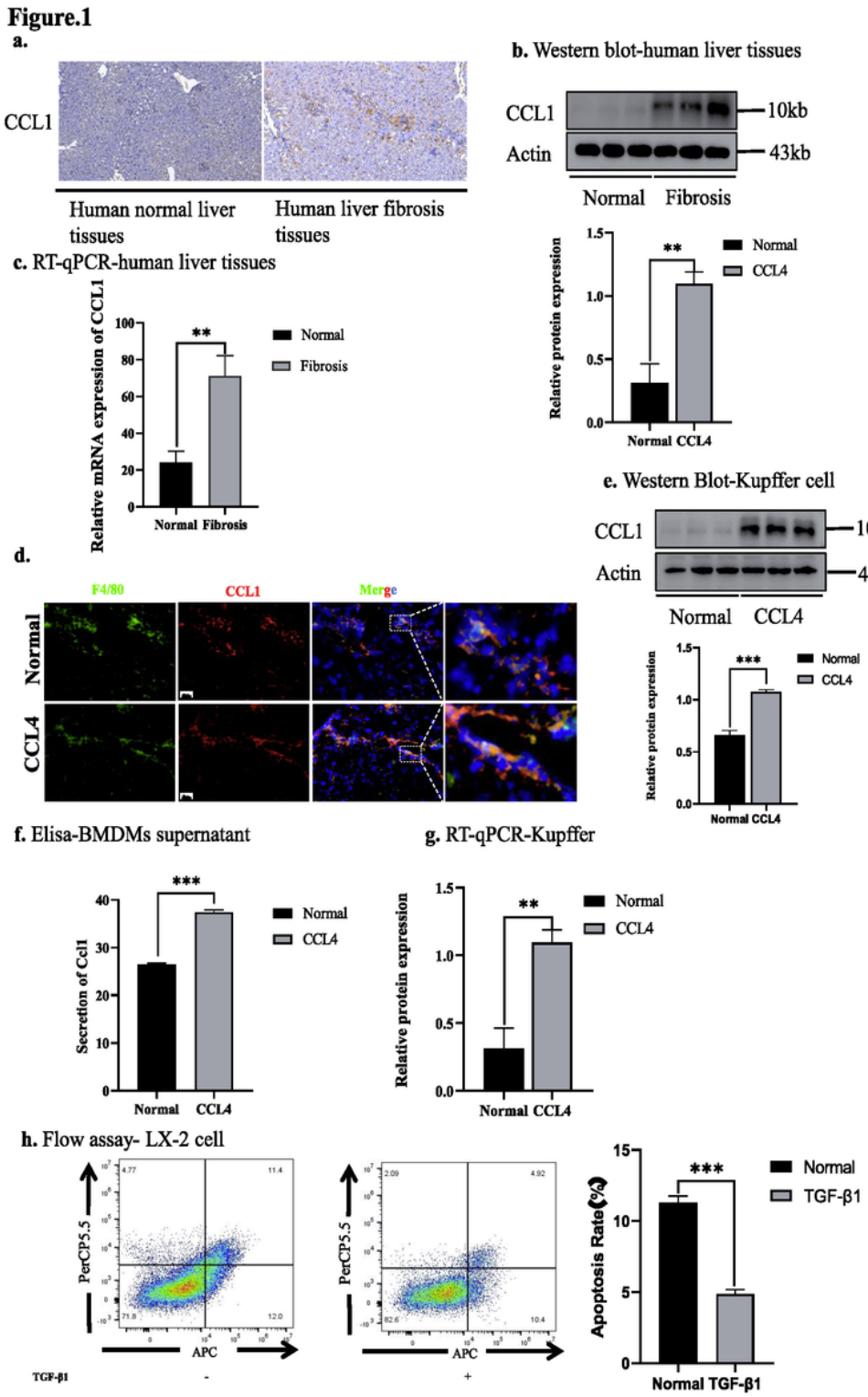


## Figure 1

CCL1 is upregulated in the liver of CCl4 model mice. (a) IHC detection of CCL1 in liver fibrotic tissue of normal and CCl4 model mice. Imaging was performed using Panorama Scan 150 (3DHISTECH, Budapest, Hungary). (b) Western blotting was used to detect CCL1 in the liver tissue of normal and liver fibrosis groups. (c) RT-qPCR was used to detect CCL1 in the liver tissues of normal and liver fibrosis groups. (d) The co-localisation of CCL1 (red) and macrophage F4/80 (green) in the liver tissue of normal

and CCl4 model mice was detected via IF. (e) CCL1 protein expression was upregulated in Kupffer cells extracted through perfusion in mice. (f) Serum CCL1 expression was increased in mice with liver fibrosis as indicated by ELISA. (g) CCL1 mRNA expression was upregulated in Kupffer cells isolated from mice. (h) APC/PerCP-Cy5.5 (7-AAD) was used as a marker for detecting the apoptosis level of LX-2 cells with or without TGF-β via flow cytometry. Data are presented as the mean ± SEM. ***P*< 0.01, ****P* < 0.001; NS, not significant.

**Figure.2**

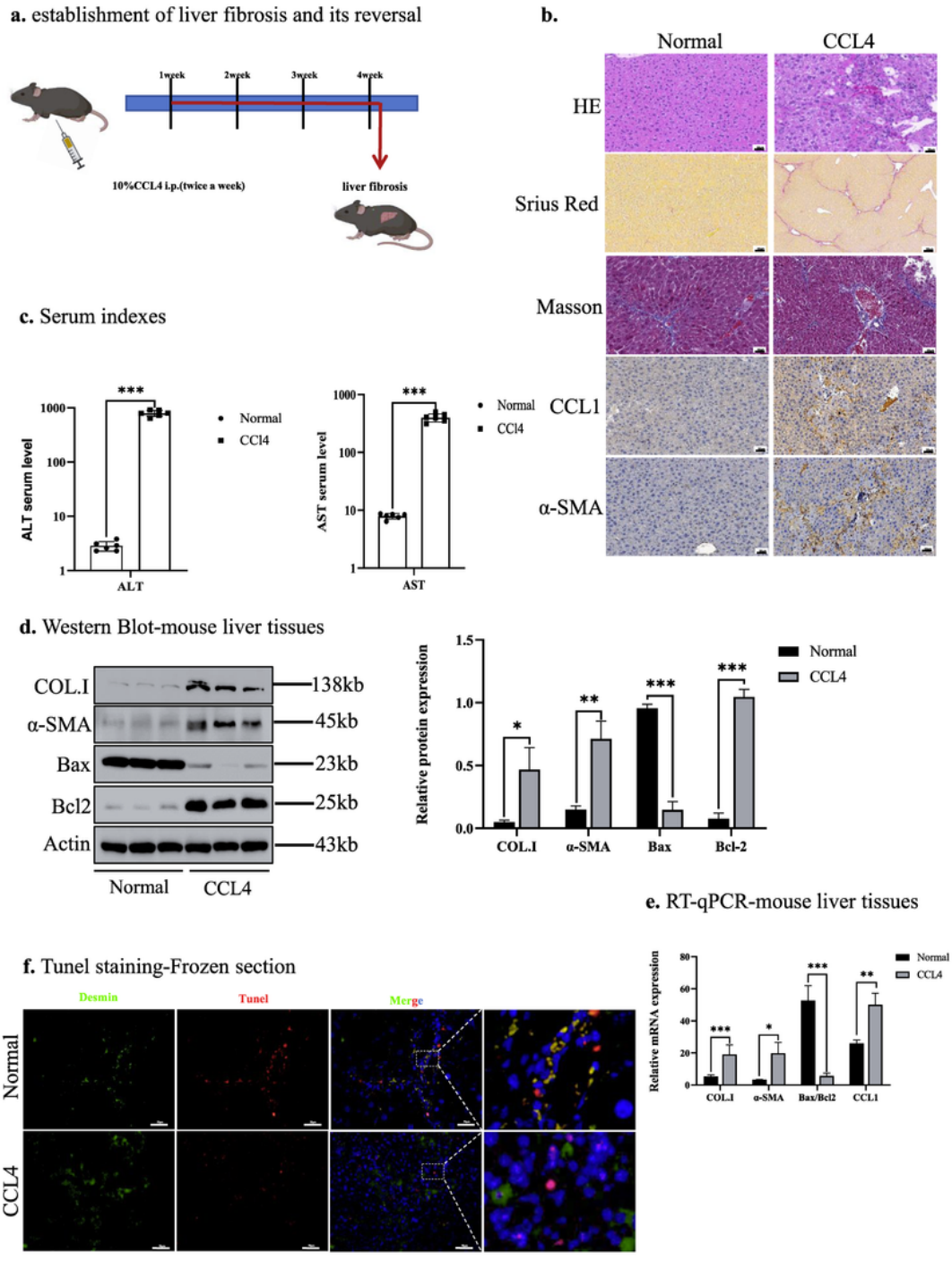

## Figure 2

(a) Successful establishment of the CCl4-induced mouse liver fibrosis model. (b) Liver tissues from mice with liver fibrosis were stained using Sirius Red, Masson's trichrome, and H&E staining, IHC-CCL1, and IHC-α-SMA. (c) The serum levels of ALT and AST were measured in both the normal group and CCl4 model mice. (d) Western blotting was used to detect the expression of Bax/Bcl-2, Col-I, and α-SMA in the liver tissue of mice in the normal and CCl4 model groups. (e) RT-qPCR was used to detect the expression of Bax/Bcl-2, Col-I, and α-SMA in the liver tissue of mice in the normal and CCl4 model groups. (f) TUNEL assay and Desmin detection via IF staining in the liver tissue of CCl4 model and normal mice. Data are presented as the mean ± SEM. $^{**}P < 0.01$, $^{***}P < 0.001$.

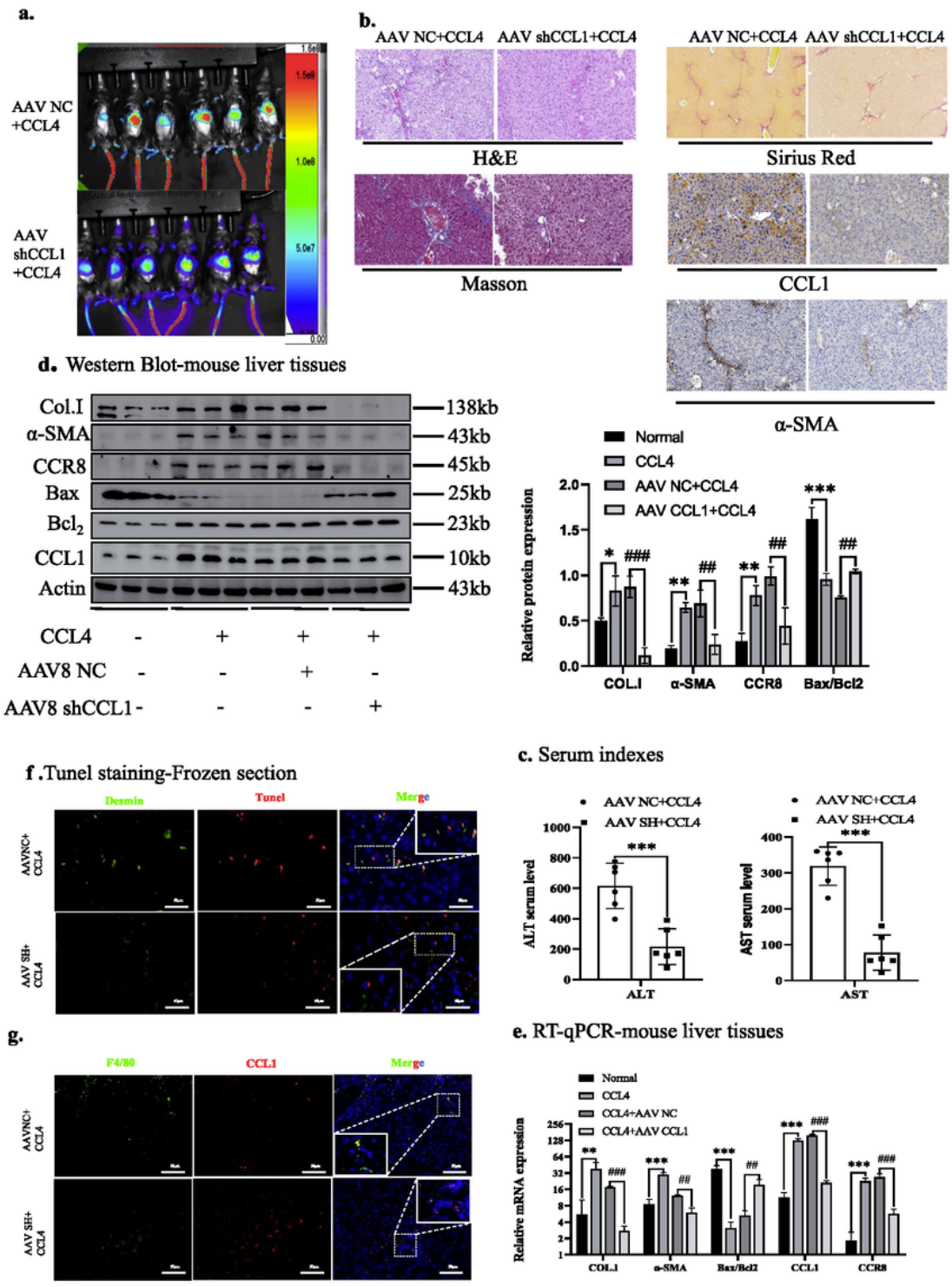


## Figure 3

Hepatic macrophage-specific AAV8-Luc-shCCL1 alleviated CCl4-induced liver fibrosis. (a) *In vivo* imaging was conducted on small animals. (b) The liver tissues of mice from the AAV-shCCL1 and AAV-NC groups were subjected to Sirius red, Masson's trichrome, and H&E staining, IHC-CCL1, and IHC-α-SMA analysis. (c) The serum levels of ALT and AST in mice from the AAV-NC and AAV-shCCL1 groups were measured. (d, e) Western blot and RT-qPCR were used to analyse the expression of CCL1, Bax/Bcl-2, Col-I, and α-SMA

in the liver tissues of mice in the AAV-NC and AAV-shTCF21 groups. (f) Co-localization of Desmin (green) and TUNEL (red) was observed in the liver tissue sections of mice from the AAV-shCCL1 and AAV-NC groups. (g) Co-localization of F4/80 (green) and CCL1 (red) in liver tissue sections of AAV-shCCL1 and AAV-NC group mice. Data are presented as the mean ± SEM. $^{**}P < 0.01$, $^{***}P < 0.001$.

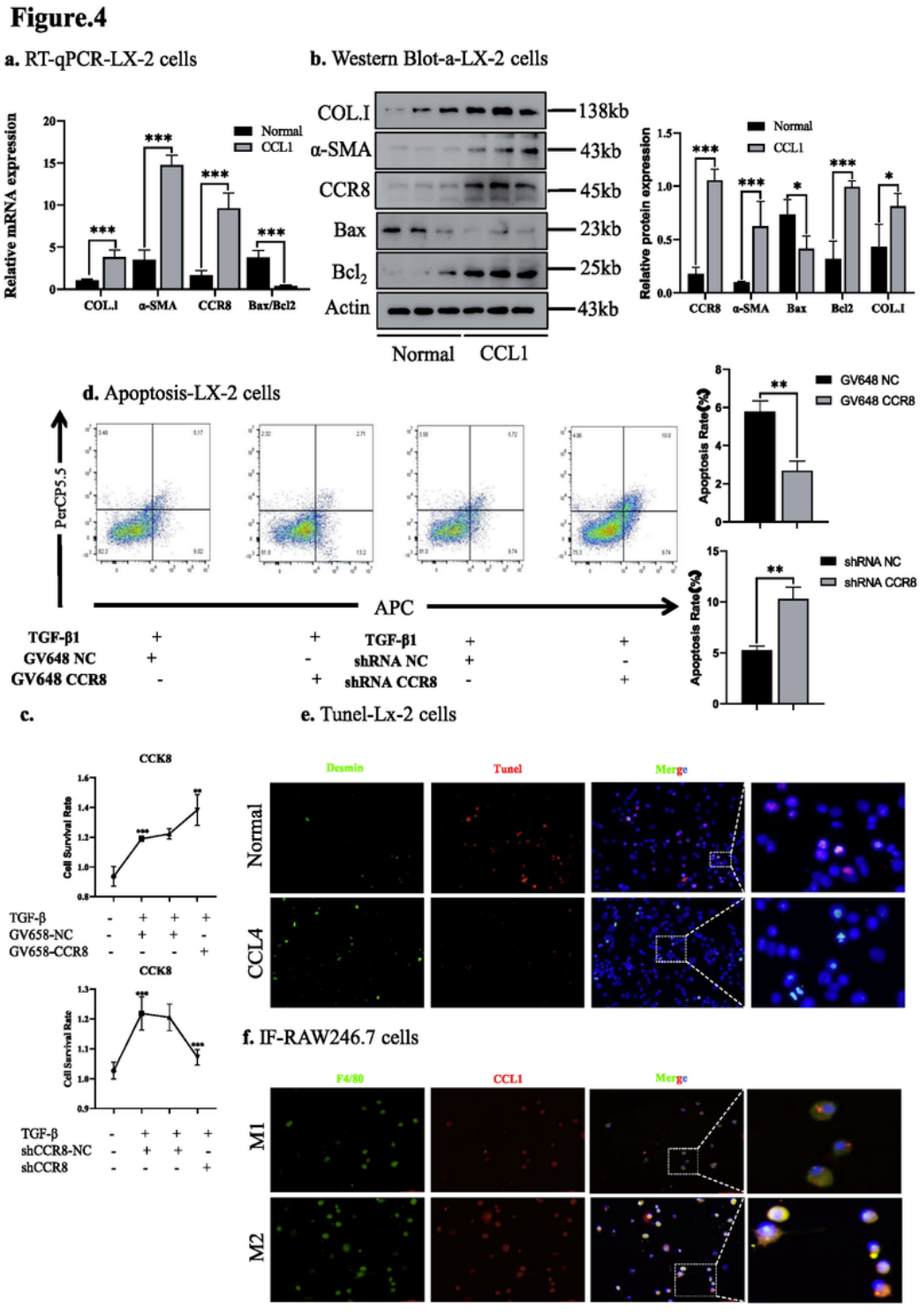


Figure 4

CCL1 affects HSC activation and apoptosis. (a) RT-qPCR was used to detect the expression levels of CCL1, α-SMA, Col-I, and Bax/Bcl-2 in LX-2 cells treated with CCL1 recombinant protein. (b) The expressions of CCL1, α-SMA, Col-I, and Bax/Bcl-2 in LX-2 cells were detected via western blotting. (c) The proliferation of CCR8-silenced or –overexpressing LX-2 cells was assessed using the CCK-8 assay. (d) Flow cytometry with APC/PercP-Cy5.5 (7-AAD) was employed to measure the apoptosis levels in LX-2 cells after silencing or overexpression of CCR8 using an apoptosis kit. Data are presented as the mean ± SEM. $^{**}P < 0.01$, $^{***}P < 0.001$.

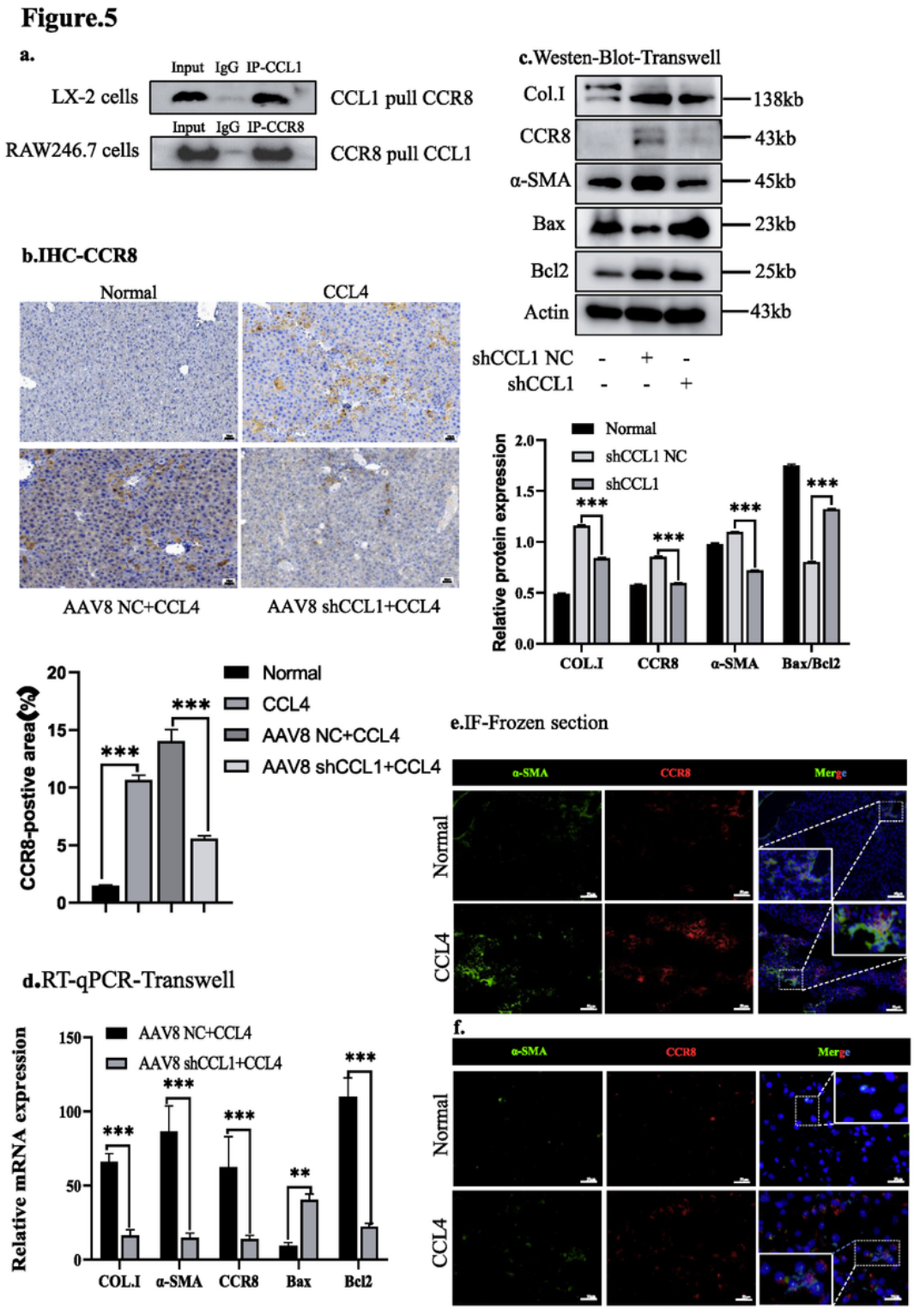

## Figure 5

CCR8 is a receptor for CCL1 on LX-2 cells. (a) The interaction of CCL1 and CCR8 proteins in LX-2 cells was detected via Co-IP. (b) IHC-CCR8 staining in AAV8-F4/80-LucNC and AAV8-F4/80-Luc-shCCL1 mice with liver fibrosis. (c) Protein expression of RAW246.7 in the control and shCCL1 groups co-cultured with mouse HSCs. (d) The mRNA expression of RAW246.7 in the control and shCCL1 groups co-cultured with mouse HSCs. (e) IF was used to observe the expression of α-SMA (green) and CCR8 (red) in liver tissues of mice with liver fibrosis and normal mice. (f) IF was used to visualize the expression of α-SMA (green) and CCR8 (red) in LX-2 cells with and without TGF-β. Data are presented as the mean ± SEM. $^{**}P < 0.01$, $^{***}P < 0.001$.

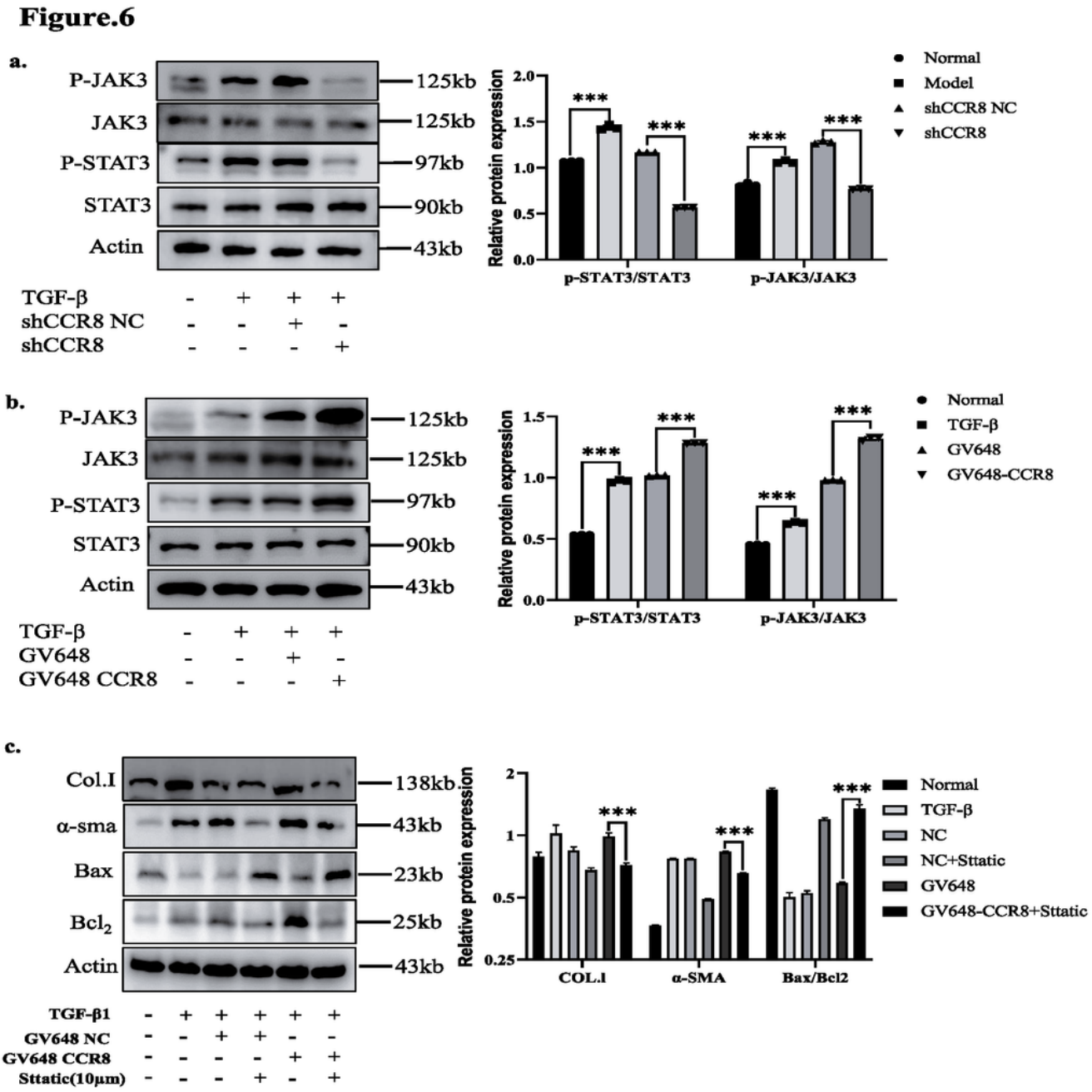


## Figure 6

CCL1 regulates the activation and apoptosis of HSCs via the CCR8-mediated activation of JAK3/STAT3. (a) The expression levels of p-JAK3/JAK and P-STAT3/STAT3 in LX-2 cells after silencing CCR8 were detected via western blotting. (b) The expression levels of p-JAK3/JAK and P-STAT3/STAT3 proteins after overexpressing CCR8 were analysed in LX-2 cells via western blotting. (c) The protein levels of α-

SMA, Col-I, and Bax/Bcl-2 were examined in LX-2 cells treated with Stattic (10 nm). Data are presented as the mean ± SEM. $^{**}P < 0.01$, $^{***}P < 0.001$.